TASHKENT STATE TECHNICAL UNIVERSITY
NAMED AFTER ISLAM KARIMOV
ISSN: 2181-0400

TECHNICAL SCIENCE AND INNOVATION

№ 3/2022

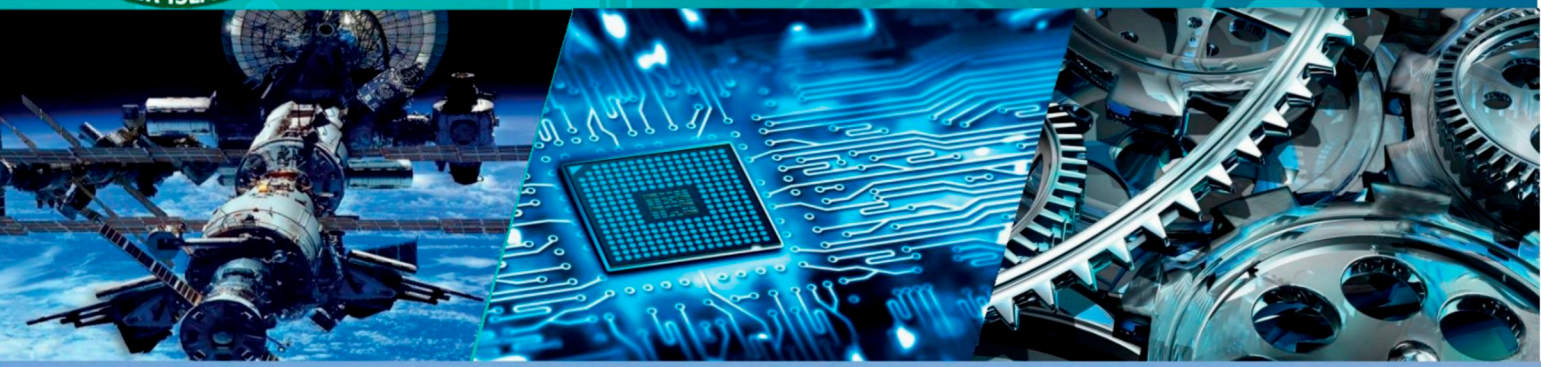

THE MINISTRY OF HIGHER AND SECONDARY-SPECIALIZED EDUCATION OF THE REPUBLIC OF UZBEKISTAN

TASHKENT STATE TECHNICAL UNIVERSITY
NAMED AFTER ISLAM KARIMOV

TECHNICAL SCIENCE AND INNOVATION

The Journal was established in 1993, Renamed in 2019

Published 4 times a year

2022, №3(13)

Tashkent 2022

the russian academy of sciences", **2003**. 168.
11. V.R. Rakhimov., A.N. Kazakov., A.R. Khasanov. Study of the stress-strain state of rocks. *"Bulletin of Tashkent State Technical University",* **2011**. 167.
12. A.V. Zubkov. "*Geomechanics and geotechnology*", **2000**. 335.
13. M.V. Kurlenya., V.M. Seryakov., A.A. Eremenko. Technogenic and geomechanical stress fields. Novosibirsk. "*Science*", **2005**. 264.
14. I.M. Petukhov., A.M. Linkov., V.S. Sidorov. Calculation methods in the mechanics of rock bursts and outbursts. "*Reference manual. Nedra*", **1992**. 256.
15. A. Markov., A. Kazakov., M. Khaqberdiyev., Sh. Muhitdinov., M. Rahimova. On the calculation of tectonic stresses in the earth's crust of South Western Uzbekistan. IOP Conference series: earth and environmental science. "*IOP Publishing*", **2021**.
16. S.G. Avershin. Mountain kicks. "*Carbontech publish*", **1969**. 210.
17. S.S. Sayyidkosimov., A.N. Kazakov. Forecast of the probility of shock hazard in conditions of underground development of Zarmitan gold deposit zones. *"Geomechanics and geodynamics of rock masses. geomechanics and geodinamiks of rock masses-selected paparis from European rock mechanics symposium Eurock",* **2018**. 499.
18. V.R. Rakhimov., M.K. Turapov., A.N. Kazakov. Forecasting rock burst hazard of deposits by modeling. "*Mining Bulletin of Uzbekistan*", **2014**. 60.

MAPPING OF MINERALS BY THE METHOD OF GEOLOGICAL INDICES FROM ASTER SPACE IMAGES

A.R.Asadov[1], A.R.Almordonov[2]
[1]University of Geological Sciences,
Olimlar st., 49 100041 Tashkent, Uzbekistan
[2]Tashkent State Technical University
Universitet st., 2.100095, Tashkent, Uzbekistan

Abstract: *The study of the spectral properties of minerals and rocks by remote sensing methods are based on mineralogical and petrographic studies. The article presents the results of calculation of mineral indices using ASTER (Advanced Space Thermal Emission and Reflection Radiometer) satellite images of the central part of the North Nurata Mountains. Pre-processing of the space image, including geometric and radiometric correction was carried out with the ENVI 5.3 program. Mineral indicators of ore minerals, such as iron oxides, carbonate, silicate and siliceous minerals were identified based on mathematical operations of ASTER space imagery channels. The mineral index results provided accurate spectral information on mineral indicator minerals and lithologic mapping while showing the spatial distribution of these materials. The areoles of the identified mineral groups mostly coincide with mineralized zones on the various ore minerals. The results can be used to create and update mineral distribution maps to predict new areas of mineral accumulations.*

Keywords: *ultispectral images, ASTER, indicator minerals, combination of channels, interpretation, mineral indices, hydrothermal alteration of rocks, gold mineralization.*

INTRODUCTION. At present, ASTER multispectral satellite images are widely used to identify and map minerals and rocks by their spectra, since they have different spectra of absorption and reflection of electromagnetic waves. Given that the indicators of ore bodies are zones of hydrothermal alteration of ore-bearing rocks, Aster multispectral satellite images allow them to be identified using geological index methods. Zones of hydrothermal alteration are closely related to most ore deposits, including gold [4]. For example, kaolinite is a common by-product associated with both gold and copper deposits. Therefore, ASTER mapping of kaolinite concentrations may indicate the presence of these ores. Proper pretreatment and combination of these bands can result in a relative distribution of mineral alterations such as iron oxides, siliceous rocks, carbonates, sericite, elite, alunite, kaolinite, etc.

The Nurata Mountains are one of the main mining regions of Uzbekistan, where most of the ore deposits and manifestations are concentrated. The purpose of this work is to study and map the halo distribution of quartz, carbonate, clay and iron-bearing tracer minerals.

MATERIAL AND METHODS. To solve the tasks set, ASTER space images were used, obtained in 14 different ranges of the electromagnetic spectrum and resolution. 4 bands using visible and near infrared (VNIR) with a resolution of 15 m, 6 bands using shortwave infrared (SWIR) with a resolution of 30 m and 5 bands using thermal infrared (TIR) with a resolution of 90 m (Fig. 1). The capture bandwidth for all sensors is 60 km.

Processing of space images was carried out in software packages ENVI (Environment for Visualizing Images) 5.3, ArcGIS 10.8. In this work, various methods were used, which are widely used in the processing of remote sensing data (RSD) [1-3; 5]. Different minerals have different spectral features in the infrared thermal region of the electromagnetic wave spectrum. These features make it possible to identify, for example, such rock-forming minerals as silicates, sulfates, and carbonates.

System	Band	Spectral range (μm)	Spatial resolution	Radiometric resolution
VNIR	1	0.52 - 0.60	15 m	8 bit
	2	0.63 - 0.69		
	3	0.78 - 0.86		
SWIR	4	1.60 - 1.70	30 m	8 bit
	5	2.145 - 2.185		
	6	2.185 - 2.225		
	7	2.235 - 2.285		
	8	2.295 - 2.365		
	9	2.360 - 2.430		
TIR	10	8.125 - 8.825	90 m	12 bit
	11	8.475 - 8.825		
	12	8.925 - 9.275		
	13	10.25 - 10.95		
	14	10.95 - 11.65		

Fig. 1 Spectral characteristics of the Aster space image

The study of the spectral properties of minerals and rocks by remote sensing methods is based on mineralogical and petrographic studies. At present, the mineral and lithological composition of the earth's crust is well known. More than 92% of the earth's crust by mass are silicates - salts of silicic acids, so their study is given so much attention. Based on the availability of technical means and the location of the spectral absorption lines of the main minerals, it was concluded that today, for spectral methods of remote sensing in geology, it is most expedient to use ASTER multispectral images [6-9]. Index imaging has long been used in the digital processing of Earth remote sensing data. To obtain it, the brightness values of each pixel are calculated by applying arithmetic operations on the brightness values of this pixel from different channels. So, there are more than two hundred vegetation indices. In geology, more than 40 such methods

have also been developed, called geological indices (mineral indices) for various remote sensing data (Fig. 2) [10-15].

Feature	Band or Ratio	Comments	Reference
Iron			
Ferric iron, Fe^{3+}	2/1		Rowan
Ferrous iron, Fe^{2+}	5/3 + 1/2		Rowan
Laterite	4/5		Bierwith
Gossan	4/2		Volesky
Ferrous Silicates (biot, chl, amph)	5/4	Fe oxide Cu-Au alteration	CSIRO
Ferric Oxides	4/3	Can be ambiguous*	CSIRO
Carbonates / Mafic Minerals			
Carbonate / Chlorite / Epidote	(7+9)/8		Rowan
Epiote / chlorite / Amphibole	(6+9)/(7+8)	Endoskarn	CSIRO
Amphibole / MgOH	(6+9)/8	Can be other MgOH or carbonate*	Hewson
Amphibole	6/8		Bierwith
Dolomite	(6+8)/7		Rowan, USGS
Carbonate	13/14	Exoskarn (cal/dolom)	Bierwith, Nimoyima, CSIRO
Silicates			
Sericite / Muscovite / Illite / Smectite	(5+7)/6	Phyllic alteration	Rowan (USGS) Hewson (CSIRO)
Alunite / Kaolinite / Pyrophyllite	(4+6)/5		Hewson (CSIRO)
Phengitic	5/6		Rowan (USGS)
Muscovite	7/6		Hewson
Kaolinite	7/5	Approximate only *	Hewson
Clay	(5x7)/(6 x 6)		Bierwith
Alteration	4/5		Volesky
Host rock	5/6		Volesky
Silica			
Quartz Rich Rocks	14/12		Rowan
Silica	(11x11)/10/12		Bierwith
Basic Degree Index (gnt, cpx, epi, chl)	12/13	Exoskarn (gnt, px)	Bierwith, CSIRO
SiO2	13/12	Same as 14/12	Palomera
SiO_2	12/13		Nimoyima
Siliceous Rocks	(11x11)/(10x12)		Nimoyima
Silica	11/10		CSIRO
Silica	11/12		CSIRO

Fig. 2 Mineral indices for the Aster satellite image

The Nurata region includes the mountains of Northern and Southern Nurata. They represent a system of uplifts and troughs plunging from SE to NW. The geological structure of Northern Nuratau is determined by intensely dislocated rocks of the Paleozoic basement, which are represented by carbonate-terrigenous strata of the Cambrian-Devonian, volcanogenic-terrigenous and sedimentary-volcanogenic strata of the Carboniferous and intrusive formations of the Carboniferous-Permian age (Fig. 3).

Paleozoic deposits are represented by: undivided Early Paleozoic deposits in the ridge. Northern and Southern Nuratau presented in the volume of the Zhivachsay and Karakush suites $Є_2$-O_1. The suite includes siltstones, sandstones, dark gray schistose, clayey inequigranular limestones and shales.

The Ordovician system is represented by the following formations: Kurbanazi (O_{1-2}kr), Dzhalatar (O_{1-2}dŽ), Ilonchisai (O_{1-2}il), Kichkinacharvak (O_{1-2}kĉ). The deposits of the Kurbanazinskaya suite are represented by mudstones, sandstones, siliceous shales, cherts and limestones. The deposits of the Dzhalatar Formation are represented by siltstones, mudstones, calcareous and siliceous shales. The Ilonchisai Formation is represented by polymictic sandstones, siltstones, and mudstones. The Kichkinacharvak Formation is represented by sandstones, siltstones, and shales.

The Silurian deposits of the Nurata region are represented by the Karatash (S_1kr), undivided Nakrut and Dzhazbulak (S_1l), Naukatsay (S_1nk) suites, and undivided deposits of the Lower (S_1) and Lower-Upper Silurian (S_{1-2}). Devonian deposits are represented by the Tulebai, Kichar and Charvak formations, which are distributed only in Northern Nuratau. Tulebai and Kicharskaya have an essentially dolomitic composition and are represented by an arbitrary alternation of

dolomites and calcareous organogenic dolomites. The Charvak suite is located in a tectonic block, represented by tuff sandstones and tuff gravelstones with lenses of dolomites and limestones.

Carboniferous deposits in the Nurata mining region are represented by the following formations: Besragatinsky (C_1bs), Syrt (C_1sr), Tababulak (C_1tb), Chambil (C_1ĉm), Predgornonurata (C_1pr), Balyklytau (C_1bl), Mikha (C_2mh), Darasai (C_2dr). The deposits of these suites are mainly represented by dacitic and andesitic tuffs, limestones, cherts, sandstones, siltstones, gravelstones, and conglomerates. The Quaternary system of the Nurata region is represented by loess-like loams with rare fragments and interlayers of crushed stone and coarser material.

The most widespread intrusive rocks within the study area are the Koshrabad gabbro, a syenite-granosyenite complex. The enclosing rocks are formations of the Dzhazbulak, Karatash and Naukatsai formations of the Lower Silurian, as well as rocks of the Kalsarinskaya, Zhivachisai and Badamchala, Nakrutskaya formations. Three subcomplexes were identified within the complex. The gabbro-syenite subcomplex includes gabbro-syenites, essexites, monzonites, syenite-monzonites of the first phase, porphyritic syenites, plagiosyenites, and quartz syenites of the second phase. The formation of the subcomplex ends with the formation of dikes of biotite-amphibole and quartz sienodiorites. The granosyenite subcomplex includes coarsely disseminated biotite-amphibole granosyenites of the first phase, finely disseminated biotite-amphibole granosyenites of the second phase, and completes it with dikes of pegmatoid amphibole-biotite granites, melanocratic syenite porphyries, and essexite porphyries. The granitoid subcomplex contains porphyritic amphibole-biotite granites of the first phase, porphyritic amphibole-biotite granites of the second phase, and vein formations are represented by dikes of aplites, granites, pegmatites, and quartz syenodiorites. The rocks of the late stage are distinguished by the stability of the mineral composition, the uniformity of textural and structural features. The petrochemical feature is high potassium alkalinity, high iron content, low magnesian content. They have an increased concentration of lithium, rubidium, barium, sfontium, fluorine, lead, very low chromium, nickel.

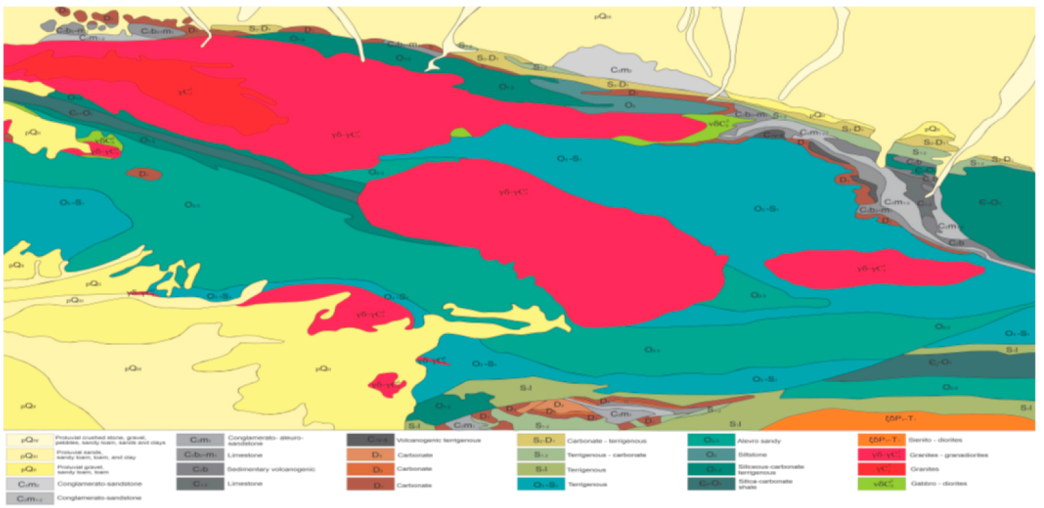

Fig. 3 Schematic geological map of the North Nurata Mountains

RESULTS AND DISCUSSION. The spectra of rocks are very diverse and are determined by the mineral composition, the type of crystal lattice of minerals, and the size of mineral grains. Especially in the infrared (near and thermal) range of the spectrum, minerals differ greatly from each other. Here, many groups of minerals, such as clays, carbonates, sulfides, have distinct absorption lines recorded by modern remote sensing equipment. Figure 4 shows the results of mapping iron oxides and hydroxides. The best results for mapping and differentiation of indicator minerals were obtained by dividing channels 1, 2, 3, 4 and 5, since these channels reflect electromagnetic radiation from ferruginous minerals more strongly than other channels.

Carbonate minerals (amphibole, chlorite, dolomite, epidote, etc.) are isolated on the basis of adding two channels of the short infrared range of the spectrum and dividing these channels. Figure 5 shows the results of the extraction of carbonate minerals. Silicate minerals (muscovite, kaolinite, sericite, alunite, etc.) are also well distinguished with the ratio of channels in the short infrared range. Figure 6 shows the results of the isolation of silicate minerals from ASTER multispectral satellite images.

Quartz minerals such as quartz, silica, etc. are released in the thermal infrared range. Figure 7 shows the results of isolation of quartz minerals. The method of processing mineral indices makes it possible to identify the areas of manifestation of various types of rocks and minerals, as well as to map their anomalously altered areas, which are an indicator of geological conditions that are promising for the discovery of mineral deposits.

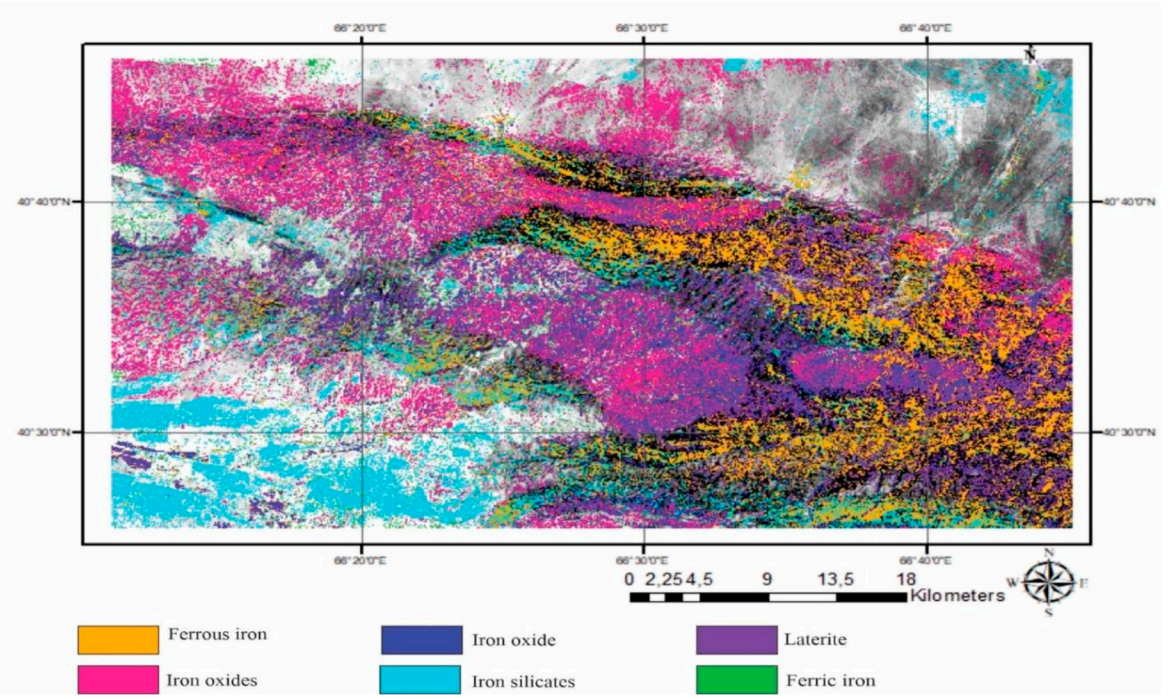

Fig. 4 Map of iron minerals

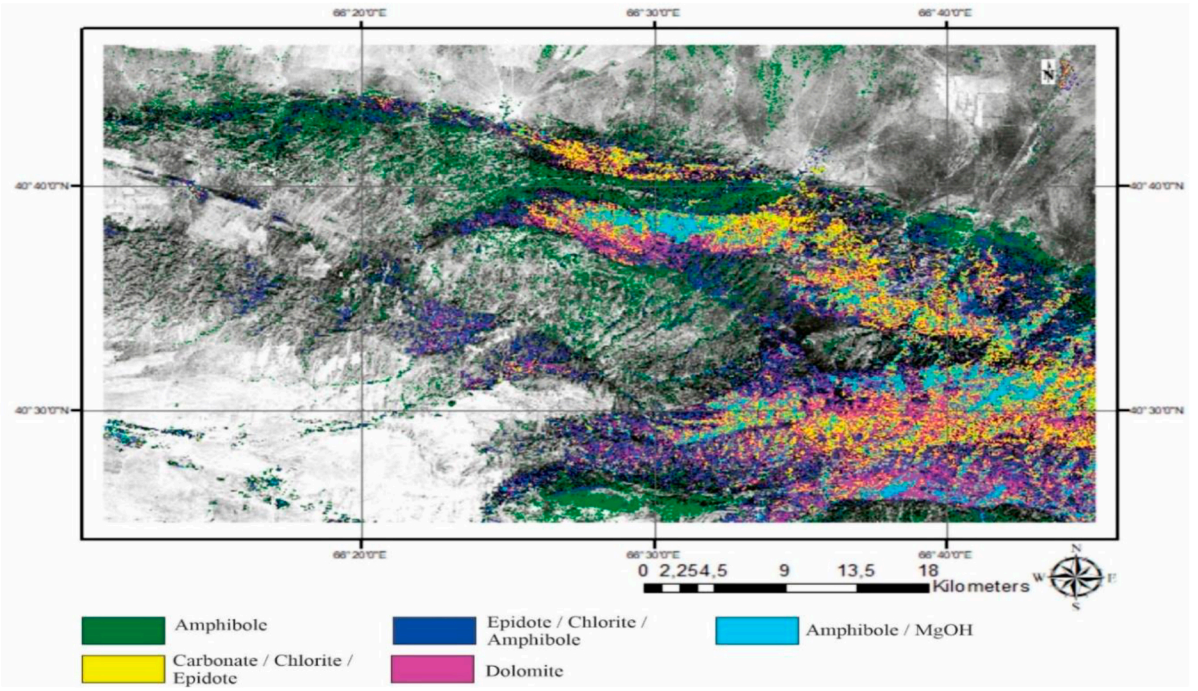

Fig. 5 Map of carbonate minerals

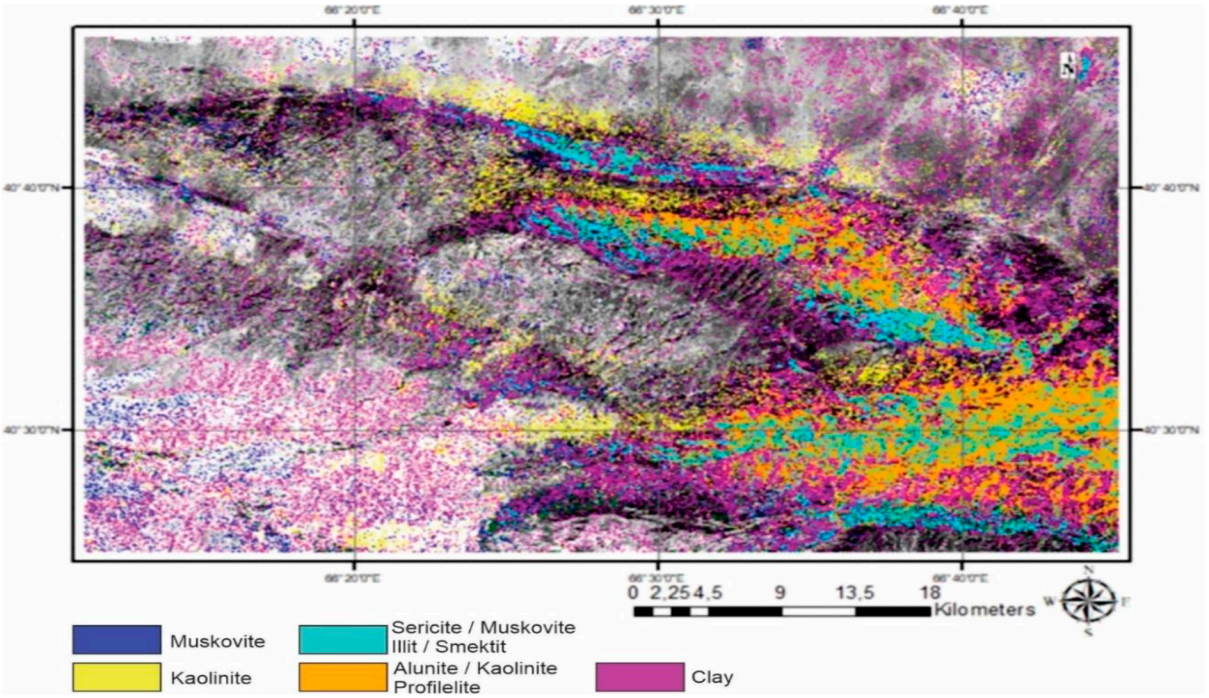

Fig. 6 Map of silicate minerals

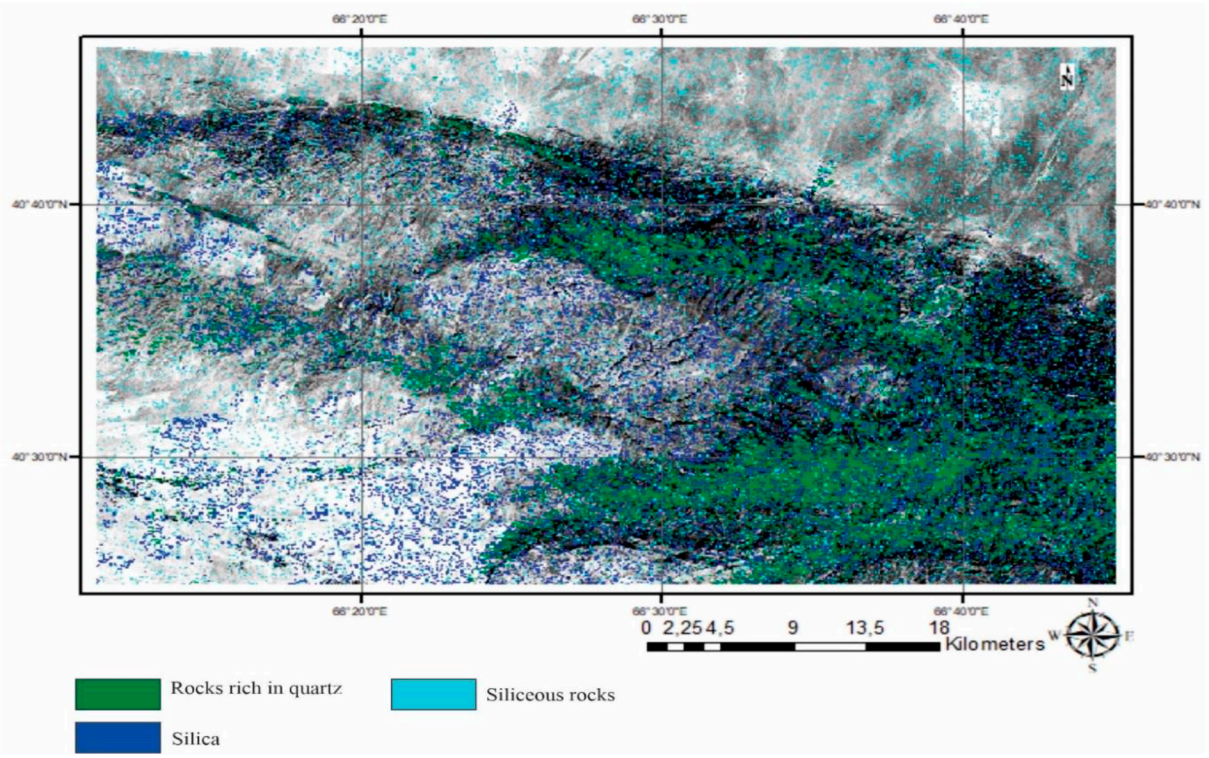

Fig. 7 Map of quartz minerals

CONCLUSION. ASTER multispectral imaging can be used effectively to detect and map ferruginous, argillaceous carbonate and quartz minerals. These minerals were found in rocks, as well as in open parts of the study area. Mineral index results have provided accurate spectral information on mineral indicator minerals and lithological mapping while showing the spatial distribution of these materials. In addition, the obtained maps of various minerals gave excellent spatial consistency and strong correlation with the geological maps of the study area. The results obtained in this work can be used to create and update a mineral distribution map in order to predict new areas of mineral accumulations.

References:

1. A.R. Asadov., A.R. Almordonov. Spectral analysis of the Landsat 8 image of the Nurata mountains by the PCA method. "*International journal of geology, earth environmental sciences",* **2021**. 227.
2. A.R.Asadov., A.R.Almordonov., S.A.Rabbimkulov., A.I.Tangirov. Identification of intrusive massifs in the Nurata mineralized zones based on satellite images. "*Technical science and innovation",* **2022**. 78.
3. A.R. Asadov., Sh. Ochilov. Calculation of mineral indices using ASTER satellite image on channel combination (by the example of the Molguzar mountains). "*Education and science in the XXI century",* **2022**.761.
4. A.A. Kirsanov. A new method for identifying near-ore hydrothermally altered rocks using space hyperspectral data, using the example of the Lomamsky potentially gold-mining region, the Republic of Sakha (Yakutia). "*Regional geology and metallogeny",* **2021**. 97.
5. A. Kanlinowski., S. Oliver. *"ASTER mineral index processing, remote sensing application, geo-science australia, internal report",* **2004.** 39.
6. Y. Zhang., F. Yao. Interpreting the Shortwave Infrared & Thermal Infrared Regions of Remote Sensed Electromagnetic Spectrum with Application for Mineral-Deposits Exploration. "*Journal of applied mathematics and physics",* **2015.** 254.
7. F. Feizi., E. Mansuri. "Separation of Alteration Zones on ASTER Data and Integration with Drainage Geochemical Maps in Soltanieh, Northern Iran. "*Open Journal of Geology",* **2013**. 134.
8. V. Henrich., A. Jung., C. Götze., C. Sandow., D. Thürkow., C. Gläßer. Development of an online indices database: Motivation, concept and implementation. 6th Easel Imaging Spectroscopy SIG Workshop Innovative "*Tool for scientific and commercial environment applications Tel Aviv*", **2009**.16.
9. V. Henrich. IDB - Index-Database; Development of a database for remote sensing indices. "*ZFL-Colloquium, Bonn",* **2012.**
10. X. Jin., S. Paswaters., H. Cline. "A comparative study of target detection algorithms for hyperspectral imagery," In Algorithms and Technologies for Multispectral, Hyperspectral and Ultra Spectral Imagery XV. *"Proceedings of SPIE",* **2014**. 7334.
11. C.I. Chang., J.M. Liu., B.C. Chieu., C.M. Wang., C.S. Lo., P.C. Chung., H. Ren., C.W. Yang., D.J. Ma. "A generalized constrained energy minimization approach to subpixel target detection for multispectral imagery. "*Optical Engineering*", **2000**.1275.
12. H. Ren., C.I Chang. "Target-constrained interference-minimized approach to subpixel target detection for hyperspectral imagery. "*Optical Engineering",* **2000**. 3138.
13. S. Johnson. "Constrained energy minimization and the target-constrained interference-minimized filter. "*Optical Engineering*", **2003**. 1850
14. S. Kraut., L.L. Scharf., R.W. Butler. "The adaptive coherence estimator: a uniformly most-powerful-invariant adaptive detection statistic. "*IEEE Trans. on Signal Processing*", **2005**. 427
15. D. Manolakis., D. Marden., G.A. Shaw. Hyperspectral image processing for automatic target detection applications. "*Lincoln Laboratory Journal",* **2003**. 79.